ResearchGate

See discussions, stats, and author profiles for this publication at: https://www.researchgate.net/publication/11568708

Structure of Hybrid Backbone Methylphosphonate DNA Heteroduplexes: Effect of R and S Stereochemistry † , ‡

ARTICLE *in* BIOCHEMISTRY · FEBRUARY 2002

Impact Factor: 3.02 · DOI: 10.1021/bi011551k · Source: PubMed

CITATIONS
23

READS
20

8 AUTHORS, INCLUDING:

David G Gorenstein
University of Texas Health Science Center at …

298 PUBLICATIONS **7,139** CITATIONS

SEE PROFILE

Available from: David G Gorenstein
Retrieved on: 24 January 2016

Structure of Hybrid Backbone Methylphosphonate DNA Heteroduplexes: Effect of R and S Stereochemistry[†,‡]

Varatharasa Thiviyanathan,[§] Katya V. Vyazovkina,[§,||,⊥] Elliott K. Gozansky,[§] Elena Bichenchova,[||,#] Tatiana V. Abramova,[||] Bruce A. Luxon,[§] Alexander V. Lebedev,[||] and David G. Gorenstein*[,§]

Sealy Center for Structural Biology and Department of Human Biological Chemistry & Genetics, University of Texas Medical Branch, Galveston, Texas 77555-1157 and Institute of Bioorganic Chemistry, Siberian Division of the Russian Academy of Sciences, 8 Lavrentyev Prospect, Novosibirsk 630090, Russia

Received July 24, 2001

ABSTRACT: Methyl phosphonate oligonucleotides have been used as antisense and antigene agents. Substitution of a methyl group for oxygen in the phosphate ester backbone introduces a new chiral center. Significant differences in physical properties and hybridization abilities are observed between the R_p and S_p diastereomers. Chirally pure methylphosphonate deoxyribooligonucleotides were synthesized, and the solution structures of duplexes formed between a single strand heptanucleotide methylphosphonate, d(Cp_{Me}-$Cp_{Me}Ap_{Me}Ap_{Me}Ap_{Me}Cp_{Me}A$), hybridized to a complementary octanucleotide, d(TpGpTpTpTpGpGpC), were studied by NMR spectroscopy. Stereochemistry at the methylphosphonate center for the heptanucleotide was either RpRpRpRpRpRp (R_p stereoisomer) or RpRpRpSpRpRp (S_p stereoisomer, although only one of the six methylphosphonate centers has the S_p stereochemistry). The results show that the methylphosphonate strands in the heteroduplexes exhibit increased dynamics relative to the DNA strand. Substitution of one chiral center from R_p to S_p has a profound effect on the hybridization ability of the methylphosphonate strand. Sugars in the phosphodiester strand exhibit $C_{2'}$ endo sugar puckering while the sugars in the methyl phosphonate strand exhibit an intermediate $C_{4'}$ endo puckering. Bases are well stacked on each other throughout the duplex. The hybridization of the methylphosphonate strand does not perturb the structure of the complementary DNA strand in the hetero duplexes. The sugar residue 5′ to the S_p chiral center shows A-form sugar puckering, with a $C_{3'}$-endo conformation. Minor groove width in the R_p stereoisomer is considerably wider, particularly at the R_p vs S_p site and is attributed to either steric interactions across the minor groove or poorer metal ion coordination within the minor groove.

Methylphosphonate oligonucleotides (MPOs)[1] are known to be attractive analogues for use as antisense, antigene, and aptamer oligonucleotides because of their nuclease resistance (*1*−*4*), easier penetration into cells due to the absence of negative charge (*1*, *5*−*7*), and ability to hybridize with complementary oligonucleotides and polynucleotides (*1*, *5*, *6*). MPOs are among the first modified oligonucleotides reported to be used as antisense molecules to inhibit protein synthesis in cell-free and cell-culture assays. Uncharged MPOs are not recognized by cellular nucleases, enter animal cells rapidly without utilizing the DNA receptors, and specifically inhibit expression of target genes, distinguishing even a single mismatch (*8*). MPOs complementary to the initiation codons of rabbit globin mRNA have been shown to inhibit globin synthesis by preventing translation (*9*), albeit not by an RNaseH hydrolytic mechanism. Reduced levels of viral DNA indicated antiviral activity of methylphosphonate oligonucleiotides complementary to the acceptor splice junction in HSV-1-infected cells (*7*). Reduction in *c-myc* and protein levels were achieved with a chimeric MPO antisense targeted to the initiation codon. However, cell proliferation was not affected (*10*). Antigene, triple-stranded-forming methylphosphonate oligonucleotides targeted to acetyltransferase mRNA, specifically inhibits protein synthesis (*11*). MPOs have also been successfully used to map the phosphate contacts that are critical for the RNA recognition by HIV-1 regulatory proteins (*12*) and to identify the critical interactions in the *trp*-repressor-operator complex (*13*).

Replacing one of the phosphoryl oxygen atoms at the phosphorus with a methyl group neutralizes the charge and introduces a new chiral phosphorus center, either in the R_p or S_p configuration (Figure 1). These two stereoisomers differ in physical properties and hybridization ability with comple-

[†] This work was supported in part by NATO Grant 931042, NIEHS (ES 04091 and ES06676), the Welch Foundation (H-1296) and the Sealy and Smith Foundation grants to D.G.G., J. Soros Grants N-RC6000 and N-RC6300 to A.V.L.. Building funds for the UTMB NMR facility were provided by NIH (1CO6CA59098).

[‡] Coordinates are available from the Protein Data Bank (PDB): 1K1R (for R isomer) and 1K1H (for S isomer).

* To whom correspondence should be addressed: E-mail david@nmr.utmb.edu. Fax: (409) 747-6850.

[§] Sealy Center for Structural Biology and Department of Human Biological Chemistry & Genetics.

[||] Institute of Bioorganic Chemistry.

[⊥] Present address: Department of Chemistry, McGill University, Montreal, PQ, Canada.

[#] Present address: School of Pharmaceutical Sciences, University of Manchester, M13 9PL, U.K.

[1] Abbreviations: DMT, dimethyl trityl; DQF−COSY, double-quantum filtered correlation spectroscopy; MP, methyl phosphonate; MPO, methyl phosphonate oligomers; PD, phosphodiester; NOESY, nuclear Overhauser effect spectroscopy; MD, molecular dynamics; r-MD, restrained MD; PME, Particle Mesh Ewald.

10.1021/bi011551k CCC: $22.00 © 2002 American Chemical Society
Published on Web 12/21/2001

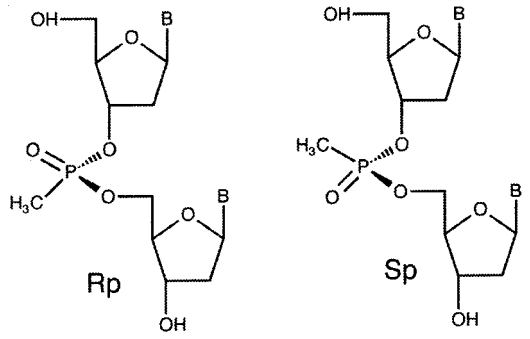

FIGURE 1: Chemical structure and stereochemistry of the R_p and S_p isomers of the methylphosphonates.

mentary DNA and RNA strands. Most studies carried out so far indicate that the R_p diastereomer forms more stable complexes as compared to S_p diastereomer (*2*, *14*−*16*). Free energy molecular dynamics decomposition calculations have indicated the origin of structural interactions and physical properties responsible for the differential stability of R_p and S_p diastereoisomers (*17*). Steric, electrostatic, and solvent interaction effects are believed to contribute to the increased stability of the R_p diastereomer. Destabilizing steric effects originate from three groups: for the S_p isomer, the C2′ and C3′ carbons (in the 5′ direction) and hydrogens unfavorably interact with the methyl group of MP, and the C5′ sugar (in the 3′ direction) carbon and hydrogen destabilize the R_p isomer. Measurements of melting temperatures of the duplexes formed by diastereomers with complementary normal DNA revealed stabilization by R_p linkages, and destabilization by S_p linkages. On the average, each substitution of a single R_p center by an S_p center in a heptamer heteroduplex DNA decreased the T_m by 3 °C. Similar results were obtained for methylphosphonate/RNA heteroduplexes (Vyazovkina and Lebedev, unpublished data).

Molecular dynamics calculations (*18*) indicated that the S_p MPOs perturb the conformations around the P−O3′ and glycosyl bonds, resulting in a decrease in stacking interactions. The R_p isomers behave similar to normal phosphate diester duplexes since the methyl group is further away from the sugar. Neither S_p nor R_p MPOs seem to significantly alter the base-paired phosphodiester conformation. Since the introduction of an MP group introduces a new chiral center, an oligonucleotide with *N* methylphosphonates will create 2^N different diastereoisomers. To increase the hybridization to target sequences for antisense or antigene applications, and minimize nonspecific effects, synthesis of diastereomerically pure MPOs is preferred.

Several methods have been reported for the synthesis and purification of stereoisomerically pure MPOs. Methods include the chromatographic separation of the diastereoisomers (*19*), block coupling of diastereomerically pure dinucleoside MPOs (*11*, *13*), and recently the kinetic resolution based on P(III) chemistry (*20*). However, almost all of these studies reported so far are on MPOs with alternating phosphate and methylphosphonate and centers. Recently we reported the synthesis of several specific diasteromers of the hetero-oligonucleoside methylphosphonate d($Cp_{Me}Cp_{Me}Ap_{Me}$-$Ap_{Me}Ap_{Me}Cp_{Me}A$) (*21*).

To better understand the effect of stereochemistry on the stability of oligonucleoside methylphosphonate duplexes, structural studies are required. Unfortunately, very little is presently known about oligonucleoside methylphosphonate structures in detail. Crystal structures of dinucleosides containing a single phosphonate center have been reported. A crystal structure of a dinucleoside d(ApT) containing S_p chiral center exhibits an unstacked, extended conformation (*22*) and d(CpG) with an R_p center exhibits a stacked conformation (*23*). Recently, a high-resolution proton NMR study of a DNA−RNA hybrid containing R_p MP centers at alternating positions in the DNA backbone was reported (*24*). It was shown that the unmodified RNA strand manifested inter-proton distances typical for A-helix. However, the DNA strand nucleosides were in neither the standard A- nor B-type conformation. The experimental data revealed that the sugar rings exhibit either an E-type conformation or a rapid conformational exchange between N- and S-type conformations. So far, no experimental data has been reported for the S_p MPOs.

There are few structures of modified backbone duplexes. For monothiophosphates, RNA/DNA hybrid backbone duplexes show little perturbation from RNA/DNA normal backbone duplexes. In contrast both monothiophosphate (*25*) and dithiophosphate DNA (*26*) mixed backbone DNA/DNA duplexes show helical distortions, forming A-like character near the thioate substitutions. The only other structural study of a duplex containing chirally pure multiple MP centers in a duplex suggested distortion by the MP, although a 3D structure was not reported (*24*).

Theoretical calculations predict higher stability for R_p diastereomeric duplexes compared to the S_p isomer, and they predict the R_p isomer to exhibit greater hybridization strength. In this paper, for the first time, using 2D NMR methods we demonstrate evidence to support the theoretical calculations that the R_p and S_p isomers exhibit different hybridization strengths. We also present the first NMR evidence to support the structural differences between two diastereomeric MPO duplexes. These are formed by individual diastereomers of heptanucleoside methylphosphonate d($Cp_{Me}Cp_{Me}Ap_{Me}Ap_{Me}$-$Ap_{Me}Cp_{Me}A$) in absolute configurations RpRpRpRpRpRp and RpRpRpSpRpRp with complementary phosphodiester octamer d(TpGpTpTpTpGpGpC). These sequences were chosen for comparison with the phosphodiester DNA duplex, d(CpCpApApApCpA)·d(TpGpTpTpTpGpGpC), used as a model oligomer in a number of physical chemical studies reported earlier (*27*).

MATERIALS AND METHODS

Synthesis of Stereospecific Diastereomers of DNA Methylphosphonate Heptamers. MPOs were synthesized based on a procedure described by Miller for solid-phase synthesis (*28*) and modified for liquid phase (*29*−*31*) using the triester method. Diastereomers of heptanucleoside MPOs were synthesized by a block coupling of diastereomerically pure MPs.

Methylphosphonic bis(imidazolide) in acetonitrile (*29*, *32*) was used as a combined phosphonylating/condensing reagent for the coupling reaction. All reactions were carried out under dry argon.

The MPO tetramer (DMT)C*p_{Me}C*p_{Me}A*p_{Me}A*(Ac) was synthesized as follows: DMT-protected MP nucleotide C* was coupled with dimer A*p_{Me}A*-Ac in Rp-configuration to yield trimer C*p_{Me}A*p_{Me}A*-Ac in R_pR_p-configuration.

Coupling of this trimer with another monomer (DMT-C*) yielded the tetramer. Diastereomers were separated from racemic mixtures using silica gel chromatography after each coupling step. The absolute configurations of the new asymmetric centers of trimer and tetramer were assigned by partial acid hydrolysis as described previously (*29*). In accordance with the results reported by us and several other groups (*4*−*6*, *21*, *29*), the R_p configuration was assigned to the fast eluting isomer.

The racemic mixture of heptamer (DMT)C*p_{Me}C*p_{Me}A*p_{Me}A*p_{Me}A*p_{Me}C*p_{Me}A*(Ac) was prepared by block coupling of individual diastereomers of tetramer ($R_pR_pR_p$-configuration) and trimer (R_pR_p -configuration). The separation of the racemic mixture of heptanucleoside methylphosphonates was done after complete deprotection and purification by RP-HPLC. Deprotection was achieved by treating with 0.5 mL of pyridine (in 80% acetic acid) at 20 °C for 60 min and an acetonitrile/water gradient was used for RP-HPLC. Affinity chromatography on a silica column (Lichrosorb-NH_2) with covalently attached complementary phosphodiester DNA, d(TpGpTpTpTpGpGpC), was used for separation (*6*). The separation was performed on a thermostated column (4 × 200 mm) using a linear gradient of increasing column temperature. The total yield after purification was 85 A_{260}U of the RpRpRpRpRpR diastereomer and 160 A_{260}U of the RpRpRpSpRpR diastereomer. Purity of the synthesized MPO strands was tested by micro column reversed-phase HPLC and ^{1}H and ^{31}P NMR. Stereospecificity of the phosphonate centers in the MPO strands was confirmed by partial hydrolysis of the strands as described earlier (*29*).

Synthesis of Deoxyribooligonucleotide. Deoxyribooligonucleotide d(TpGpTpTpTpGpGpC) was synthesized by the triester method in the liquid phase with the use of standard reagents: 2,4,6-triisopropylbenzenesulfonyl chloride and 1-methylimidazole. After complete deprotection using dilute ammonia (30 min) and diethylenediamine (8 h at room temperature) (*33*), oligonucleotides were purified by ion-exchange and RP-HPLC. All reactions were carried out under dry argon, and the solvents were distilled from calcium hydride.

UV Melting Experiments. Melting experiments were carried out using a custom-made microscale instrument based on the Milichrom-2 spectrophotometric detector (PO-Nauchpribor, Orel, Russia). Stoichiometric amounts of component oligomers, calculated from optical density measurements, were mixed and dissolved in a buffer containing 10 mM sodium phosphate (pH 7.0), 1 mM EDTA, and either 100 mM or 1 M NaCl. Concentration of the double-stranded DNA duplex was 15 μM. Samples were heated from 2 to 80 °C at a rate of approximately 0.5 °C/min, and the absorbance (at 280 nm) was recorded approximately every 0.2 °C. Melting temperatures were determined as the maximum point on the first derivative (d*A*/d*T*) vs temperature (*T*) curves.

NMR Samples Preparation. For both samples, an equimolar ratio mixture (calculated using optical density measurements) of the two component strands, d(Cp_{Me}Cp_{Me}Ap_{Me}Ap_{Me}Ap_{Me}Cp_{Me}A) and d(TpGpTpTpTpGpGpC) (with the methylphosphonate chain in configuration $R_pR_pR_pR_pR_pR$ or $R_pR_pR_pS_pR_pR$) were mixed together, and the stoichiometric ratio was monitored by the integration of NMR signals of protons from each strand. The complexes were prepared by dissolving lyophilized oligonucleotides in the following buffer: 100 mM NaCl, 10 mM NaH_2PO_4/Na_2HPO_4, 0.1 mM EDTA, pH 7, prepared in 99.9% ^2H_2O. The final concentrations of samples were 1.8 mM for the duplex of $R_pR_pR_pR_pR_pR$-diastereomer and 2.2 mM for the duplex of $R_pR_pR_pS_pR_pR$-diastereomer. TSP was used as an internal standard and set to 0.00 ppm for all temperatures studied. In this paper, the heteroduplex containing all R_p chiral centers will be referred as the R_p isomer, and the duplex with the fifth position substituted with S_p center will be referred to as the S_p isomer (even though it has only one S_p center, all others being R_p isomers).

NMR Experiments and Data Analysis. One- and two-dimensional proton and phosphorus NMR spectra were recorded with the two MPO samples. Two-dimensional proton NOESY and TOCSY experiments were acquired at 750 MHz on Varian UnityPlus instrument equipped with pulsed field gradients. Two-dimensional NOESY data were collected in hypercomplex mode (*34*) at different NOE mixing times (from 80 to 500 ms) and at different temperatures (from 5 to 35 °C). The acquisition parameters for the 2D NOESY experiments were as follows: 7900 Hz spectral width, 5 s relaxation delay, 0.26 s acquisition time, 8 scans/increment, and 512 t_1 increments. Two-dimensional TOCSY spectra were recorded with 30 and 80 ms spin-locking mixing times at 5, 15, and 25 °C, with 2048 × 512 points and a spectral width of 7600 Hz in both dimensions. The relaxation delay was 6 s. DQF−COSY experiments were acquired at 600 MHz under hypercomplex phase-sensitive mode (*35*). A homospoil (HS-90-HS) pulse was applied at the beginning of the pulse-sequence to compensate for the short relaxation delay time. One- and two-dimensional NOESY data were collected on the samples in H_2O to observe the amino and imino exchangeable protons. One-dimensional proton spectra in H_2O were collected as a function of temperature. One-dimensional phosphorus and two-dimensional ^{1}H-^{31}P HMBC experiments were done at 162 and 240 MHz on Varian UnityPlus instruments using either a broadband Nalorac or Varian probe optimized for phosphorus and proton detection. Acquisition parameters for the two-dimensional ^{1}H-^{31}P HMBC experiment were 256 increments with 16 scans/increment and 2K points, 6269 Hz sweep width, and 1.8 s relaxation delay. One-dimensional phosphorus spectra were collected with 34K points and 256 scans, and a spectral window of 26 936 Hz. All NMR data were processed using VNMR (Varian) software. The NOESY and TOCSY data were processed with 90° shifted sign bell apodization function in both dimensions. A sine bell deconvolution function was used to suppress the residual HOD signal. The time domain data were zero-filled to increase spectral resolution in both dimensions.

Distance Calculations and Structure Refinement. Starting model coordinates were constructed using the xLEAP suite in the molecular mechanics/dynamics program AMBER5.0 (*36*) and were subjected to energy minimization to remove any unfavorable van der Waals contacts. The starting structure was placed in a rectangular box, providing at least 10 Å of explicit TIP3P water molecules (*37*) around each DNA yielding approximately 4692 water molecules. To neutralize the negative charges on phosphates, 8 Na^+ ions were placed around the charged phosphate groups in the phosphodiester strand. Constant pressure was maintained

with isotropic scaling. The water box was first subjected to a series of equilibration MD runs while holding the solute fixed (*38*). Position constraints on solute molecules were gradually relaxed during the equilibration steps as well as the final refinement runs. These steps were performed using the particle mesh Ewald (PME) method to calculate electrostatic interactions (*39*). The resulting structure was used as the starting structure for the subsequent rounds of refinement using r-MD.

Inter-proton distances were derived from the integrated 2D NOESY cross-peak volumes using the hybrid, complete relaxation matrix program MORASS (*40*, *41*). NOE spectra were simulated from starting model structures at 200 ms mixing time assuming an isotropic correlation time of 2.8 ns. This assumption is validated by previous calculations (*42*) that indicated that linear DNA molecules with less than 13 base pairs behave isotropically. A hybrid of experimentally determined NOESY cross-peak volumes and calculated NOESY volume matrix of starting geometry was built to approximate a complete experimental NOESY volume matrix. The cross relaxation rate for each proton pair was then calculated with multiple spin effects explicitly treated. Inter-proton distances were calculated from the cross-relaxation rates assuming a simple isotropic spectral density function.

Structure refinement was carried out in an iterative cycle using a pertubational merging of experimental NOESY volumes with the theoretical volume matrix (*40*, *41*). Approximately 50% of the available experimental volumes were merged in the first iterative cycle and the amount merged at each subsequent step was increased by 10−15% until the experimental data was completely merged.

The errors (i.e., uncertainties) in the calculated proton−proton distances were described using a flat-well energy penalty function in which the width of the flat-well is defined as a percentage of the equilibrium interproton distance, $\mathbf{r}_{ij}^{eq}$. For each of the starting structures the flat-well span was decreased from an initial value of ±25% $\mathbf{r}_{ij}^{eq}$ to ca. 10% while the distance restraint force constants were increased accordingly as the structures approached convergence.

To ensure Watson−Crick base-pairing in the helix, hydrogen bond restraints at an equilibrium distance of 1.9 Å (±0.19 Å) were added between the base pairs. The force constant on each hydrogen bond restraint was 15 kcal/mol Å^2. Only one hydrogen bond restraint was applied to either AT (between N1 of A and H3 of T) or GC base pairs (between H1 of G and N3 of C) to allow propeller twist between the base pairs during the refinement.

During r-MD, the nonbonded interaction cutoff distance was set to 10 Å and a distance-dependent dielectric constant was used with an integration time step of 1 fs. Coordinates were stored every 50 steps. The charges at the 5′ and 3′ ends of the DNA strands were modified to avoid nonphysical electrostatic interactions.

For each iteration, the starting structure was first energy minimized against the NOE restraints for 3000 steps followed by 8 ps of r-MD with temperature annealing (increased the temperature from 298 to 600 K for 2 ps, cooled to 298 K over the next 3 ps, continued at 298 K for the last 3 ps). The average structure from the last 3 ps of r-MD was energy minimized, and the resulting structure was used as the starting structure for the next iteration of MORASS/r-MD.

Table 1: Melting Temperatures of the Duplexes of Individual Diastereomers of Methylphosphonate Heptamer d(CCAAACA) with Complementary DNA; d(TGTTTGGC)

	T_m (°C)	
diastereomer[a]	0.1 M NaCl	1 M NaCl
RRRRRR	30.5	28
RRRSRR	27	
RSRRRS	25	24
RSRSRS	23	
SRSRSR	14.5	15
SRSSSR	13	
SSSRSS	13.5	14
SSSSSS	12.5	
d(CCAAACA)	21	35

[a] Only absolute configurations of asymmetric phosphonate centers are shown.

The progress of the iterative refinement process to convergence was monitored by several key indicators. The rms error in the volumes was used as the first criteria for monitoring the refinements. The % rms(volume) is given by

$$\%\ \text{rms (volume)} = \sqrt{1/N \sum_{ij} \left(\frac{v_{ij}^a - v_{ij}^b}{v_{ij}^a} \right)^2} \times 100\%$$

where *a* or *b* can be either the experimental or theoretical 2D volumes to give the % rms(exp) or % rms(the), respectively.

An *R*-factor, similar to the *R*-factor used in X-ray crystallography, was also used as a refinement criterion. The *R*-factor is given by

$$R = \frac{\sum_{ij} |v_{ij}^a - v_{ij}^b|}{\sum_{ij} v_{ij}^a}$$

We have suggested that the % rms(volume) is a very useful measure of quality of fit to the spectra since it weighs the percentage differences in the theoretical and experimental volumes for both large and small cross-peaks equally. Thus, the % rms(volume) is more sensitive to weaker cross-peaks which correspond to longer range (e.g., interresidue) distances. The *R*-factor is regarded as a poorer measure of the quality of the refined structure since it is often dominated by the largest cross-peaks. Another figure of merit for the quality of fit, the *Q*(1/6) factor (*43*), also appears to better reflect the quality of the structure since it weighs the weak cross-peaks more heavily than the *R*-factor. The *Q*(1/6) factor is defined as

$$Q(1/6) = \frac{\sum_{ij} \tau_m |(v_{ij}^a)^{1/6} - (v_{ij}^b)^{1/6}|}{\sum_{ij} (1/2) \tau_m |(v_{ij}^a)^{1/6} + (v_{ij}^b)^{1/6}|}$$

RESULTS

Measurements of Melting Temperatures. The melting temperatures were determined as the maximum points of the first derivative plots and are shown in Table 1. For the PD

DNA duplex, the melting temperature showed significant increase when the NaCl concentration was increased from 0.1 to 1.0 M. However, the melting temperatures did not change significantly for the hetero-duplexes containing MPOs, when the salt concentration is increased. The results in Table 1 also show that the substitution of S_p center for an R_p center reduces the melting temperature of the hetero duplex. Along with the number of the S_p substitutions, the position of the S_p substitution also plays a significant role in determining the melting temperature of the duplex. A sharp, significant increase in T_m for the duplex with SRSRSR (14.5°) compared to the duplex of RSRSRS (23°) implies a structural transition. In pyrimidines, the substitution at C5 is in close proximity to the S-methyl group (of the phosphonate) resulting in an adverse steric effect (*17*). In the SRSRSR, there would be two cytosines with S_p centers whereas in the RSRSRS, there are no cytosines with S_p conformation, resulting in the formation of a more stable complex. This may explain the increase in T_m between these two complexes. In 100 mM NaCl, the all-R_p MPO heptamer was significantly more stable in a duplex with complementary DNA than the PD DNA duplex. These results show that it is possible for the all-R $_p$ MPO diastereomers to invade a duplex PD DNA, as was the results found for the polyamide DNA (*44*). As would be expected for a neutral oligomer, the melting temperatures for MPOs showed little dependence on salt concentration.

Assignment of Nonexchangeable Protons. Due to the loss of signal intensity at higher temperatures, the NOE spectra collected at 5 °C were used to make sequential assignments. Nonexchangeable protons were assigned using the established sequential assignment strategy for nucleic acids (*45*) and are reported in Table 2. Although neither an A-form nor B-form-type geometry was initially assumed, the sequential assignment of this duplex followed that for a right-handed helix.

Sequential assignments were based on the aromatic−H1′ connectivities and were confirmed by the aromatic−aromatic cross-peaks and aromatic-H2′/H2″/H3′ connectivities. Inter-residue NOESY cross-peaks from the H5 of pyrimidines to the H6/H8 base proton of the (i−1) residue were also present. Other sugar protons (H3′, H4′, H5′, and H5″) were independently assigned from the 2D NOESY and DQF−COSY (and 2D TOCSY) spectra. The 50 ms mixing time NOE spectra were used to confirm the assignments of the sugar protons using the intra-sugar NOESY cross-peaks. The assignments of individual sugar protons were confirmed by the relative intensities of the intra-sugar cross-peaks in the 50 ms NOESY spectra. Weak sequential H1′(n)→H1′(n+1) connectivities were also observed and were used to confirm the H1′ assignments. Sugar H2′ and H2″ resonances were assigned by comparing the intensities of intra-sugar NOEs. Sugar H2′ proton is closer to the H1′ of the same sugar than any other protons irrespective of the sugar pucker. The H1′−H4′ distance is shorter than the H1′−H3′ distances, irrespective of the sugar pucker. The H4′−H5′/H5″ scalar cross-peaks were either overlapped or too weak to be seen due to small coupling constants (less than 3 Hz). Stereospecific assignments for the H5′/H5″ were not made. However, it is assumed that the H5′ resonate downfield from the H5″ (*46*).

The H2 resonances of adenines were assigned by their strong cross strand NOESY cross-peaks to base-paired imino protons of thymidines and by their sequential NOESY cross-peaks to the H1′ of the 3′ residue.

Table 2

residue	H8/H6	H5/H2/Me	H1′	H2″	H2′	H3′	H4′	P[a]
Assignment of Chemical Shifts for the S-isomer (5° C)								
T1	7.61	1.77	5.79	2.20	2.42	4.85	4.22	
G2	8.08		6.11	2.76	2.89	5.02	4.46	−0.78
T3	7.41	1.42	6.19	2.27	2.64	4.94	4.34	−0.93[b]
T4	7.54	1.72	6.17	2.21	2.62	4.92	4.17	−1.25
T5	7.40	1.72	5.69	2.06	2.32	4.88	4.11	−0.99
G6	7.89	-	5.56	2.69	2.69	5.00	4.34	−1.36
G7	7.81	-	6.01	2.53	2.58	4.95	4.38	−1.06[b]
C8	7.76	5.91	6.24	2.27	2.35	4.55	4.12	−0.53
C9	7.60	5.71	5.97	2.15	2.39	4.98	4.16	
C10	7.44	5.73	5.36	2.00	2.10	5.06	4.19	35.81
A11	8.16	7.62	5.96	2.69	2.83	5.38	4.47	36.03
A12	8.18	7.44	5.46	2.68	2.73	5.30	4.25	35.95
A13	7.99	7.27	6.09	2.57	2.68	5.33	4.53	36.28
C14	7.09	5.19	5.71	1.74	2.15	4.98	4.27	35.75
A15	8.12		6.27	2.43	2.66	4.65	4.21	35.72
Assignment of Chemical Shifts for the R-Isomer (5 °C)								
T1	7.63	1.79	5.84	2.25	2.44	4.86	4.22	
G2	8.09		6.13	2.78	2.93	5.02	4.45	−0.73
T3	7.44	1.43	6.22	2.37	2.69	4.95	4.37	−1.03
T4	7.58	1.67	6.19	2.27	2.65	4.94	4.23	−1.24
T5	7.38	1.74	5.80	2.06	2.35	4.88	4.12	−0.89
G6	7.93		5.51	2.69	2.69	5.01	4.37	−1.31
G7	7.87		6.07	2.61	2.68	4.97	4.42	−0.96
C8	7.74	5.85	6.22	2.25	2.33	4.55	4.10	−0.61
C9	7.64	5.86	5.97	2.15	2.39	5.01	4.16	
C10	7.48	5.76	5.38	2.03	2.13	5.06	4.19	35.74
A11	8.28		5.87	2.69	2.90	5.39	4.52	35.55
A12	8.16		5.99	2.75	2.79	5.28	4.55	35.92
A13	8.04		6.07	2.57	2.71	5.28	4.53	35.82
C14	7.09	5.19	5.71	1.74	2.16	4.98	4.29	35.48
A15	8.12		6.29	2.41	2.66	4.65	4.21	36.10

[a] Assignment of P on the 5′ side of the residue. [b] These two assignments are ambiguous.

From the chemical shifts listed in Table 2, it can be noted that the chemical shifts of H3′ protons for the sugars in the MPO strands (for both duplexes) are shifted downfield compared to the H3′ shifts in the phosphodiester strand. Similar results were reported for hetero-duplexes containing phosphorothioate and phosphorodithioate strands (*47*). The chemical shifts of H4′ protons of the MPO strand also shifted downfield compared to the H4′ protons of PD strand. Since the H3′ and H4′ protons are closer to the backbone MP group compared to the other sugar protons, the downfield shift may be attributed to the presence of methyl group in the phosphonate backbone.

The methyl protons of the MP group were assigned using the ^{1}H-^{31}P HMBC spectra. These methyl protons showed NOESY cross-peaks to the H3′ and H4′ protons on the 5′ side of the phosphonate groups and H5′/H5″ protons and weak NOESY cross-peaks to the H3′ protons on the 3′ side. In the case of the S_p isomer, a strong NOESY cross-peak was observed between the methyl group of A12 and the H3′ of A13, suggesting that this inter-proton distance is shorter for S_p isomers compared to the distance found in R_p isomers.

Exchangeable Proton Assignments. The amino and imino protons were assigned from the 1D and 2D spectra collected in H_2O. In the 1D spectra collected as a function of temperature, the imino signals disappear for both R_p and S_p samples above 10 °C. For the S_p isomer, 5 imino proton signals were observed at 5 °C. The imino protons of G6 and

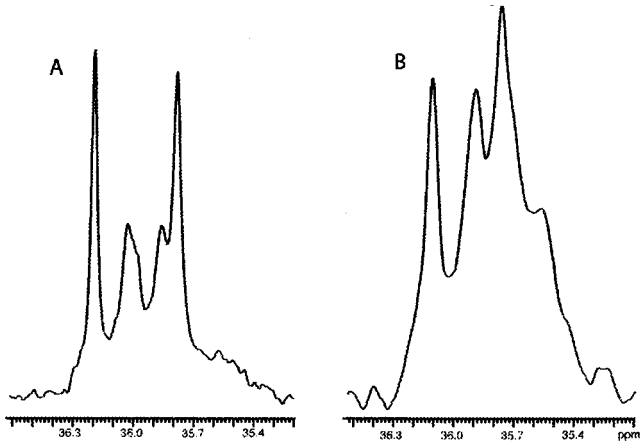

FIGURE 2: One-dimensional ^{31}P NMR spectra of (a) S_p and (b) R_p isomer heteroduplexes. Only the phosphonate region of the spectra is shown. The ^{31}P spectra were collected at 162 MHz and at 25 °C. Chemical shifts are referenced to 85% H_3PO_4 at 0.0 ppm.

G7 residues were not seen. At 8 °C, the imino proton of the T1 residue disappears, and all imino signals disappeared at 15 °C. In the case of R_p isomer, at 8 °C all but the imino proton of G7 was observed. At 15 °C, imino protons of G2, T3, T4, and T5 were seen. All imino signals disappeared at 23 °C. Three strong inter-strand NOESY peaks were observed between T-imino protons and the H2 protons of the base-paired adenines. The NOESY cross-peak corresponding to the terminal A:T basepair was not observed.

Assignment of Phosphorus Resonances. ^{31}P chemical shifts were assigned from the 2D HMBC spectra based on the H3′ and H4′ sugar resonance assignments. The methyl groups of the MP were also identified using the HMBC experiment, as the ^{31}P-^{1}H coupling in MP is around 17 Hz.

The ^{1}H-^{31}P HMBC spectrum showed six peaks in the methyl region. The NOESY cross-peaks between the sugar H3′/H4′ and the methyl protons in the phosphonate group were differentiated by their characteristic splitting (of 17 Hz) due to the adjacent phosphorus attached to the methyl group. The ^{31}P spectra were referenced to 85% phosphoric acid at 0.0 ppm, which is 3.45 ppm upfield of trimethyl phosphate (TMP). The ^{31}P signals of the phosphate diesters resonate between −1.4 and −0.5 ppm. At all temperatures, the ^{31}P chemical shifts of the phosphodiesters are dispersed within this 0.9 ppm range, which is typical for normal B_I conformation (*48*). The methylphosphonate phosphorus resonates downfield between 35 and 37 ppm. The phosphorus of the S_p phosphonate center resonates further downfield compared to the phosphorus atoms in the R_p MP (Figure 2).

The downfield shift of phosphorus resonances of phosphate diester oligonucleotides are interpreted as an indication that the phosphates contain a higher population of trans, P−O3′ torsional angle, ϵ (*48*). While such a correlation has not been established for the phosphonates, the downfield shift of the ^{31}P resonance suggests that the S_p phosphonate may exist more frequently in a B_{II} (ϵ = trans) conformation. Molecular mechanics calculations also revealed that the presence of S_p introduced a certain degree of restriction for the P−O3′ rotation with an increase in the barrier for the B_I-B_{II} transitions (*18*).

Sugar Puckering and Glycosidic Torsional Angles. The 2D TOCSY spectra collected at 5 °C were used to assign the sugar spin systems of each residue. The H1′−H2′ and H1′−H2″ scalar cross-peaks were observed for both the phosphodiester and MP strands, suggesting that the sugars in both strands exhibit B-form sugar puckering. However, for the A-12 residue of the S_p isomer, the H1′/H2′ cross-peak is very weak, indicating this residue shows some A-form characteristics. The relative intensities of the NOESY cross-peaks of intra and interresidue H8/H6 to H2′ and H2″ further support the conclusion that the sugar residues in the PD and MPO strands exhibit B-form sugar puckering while the puckering is reversed for the A12 residue of the S_p isomer sample. For the sugar residues in the MPO strand, scalar peaks of equal intensity were observed between H2′−H3′ and H2″−H3′, indicating that these sugars exhibit C_4′ endo or O_1′ endo sugar puckering with a pseudorotation angle (*P*) around 70°.

Coupling constants for the sugar protons were estimated from the DQF−COSY spectra collected at 5 °C for both the R_p and the S_p isomers. The coupling constants between the H2′ and H3′ and the H2″ and H3′ protons also support the C_4′-endo sugar puckering in the MPO strand. On the basis of the intensity of the NOESY cross-peaks between H8/H6 and their own H1′ protons, it was determined that the glycosidic torsional angles are anti for all the residues, and none exhibit a syn conformation.

Two-Dimensional NOESY as a Function of Temperature. Sequential H8/H6→H1′ NOESY connectivities were observed for both phosphodiester and MPO strands for both isomers at 5 °C. The NOESY cross-peaks were sharp and strong with the expected connectivity. However, as the temperature increased, the sequential NOESY connectivites for the MPO strand disappears, while the connectivities remain for the phosphodiester strand. The H8/H6−H1′ region of the NOE spectra collected at different temperatures is shown in Figure 3. Normally, as the temperature of a nucleic acid duplex is raised close to the melting temperature, there would be a general loss of NOESY connectivity—this is consistent with increased flexibility, increased populations of multiple conformations, and thus diminition of NOE volumes. The R_p isomer showed loss of connectivity at the ends of the MPO strand consistent with end-fraying with temperatures that approach the melting temperature of 30 °C. However, the PD strand did not show as much loss of connectivity as expected. Even at 25 °C there remained significant connectivity and cross-peak intensity in the central region of the PD strand while no stable connectivity was detected in the MPO strand. For the R_p isomer, the NOESY connectivities in MPO strand disappear at 20 °C. This differential loss of NOESY connectivity within the PD and MPO strands is even more pronounced for the S_p isomer. The S_p isomer, which has a melting temperature about 10 °C lower than the R_p isomer, begins to lose NOESY connectivity in the MPO strand between 10 and 15 °C. Also, the MPO strand cross-peaks had larger line widths than the PD strand, suggesting an increased conformational flexibility.

Accounting for the premature loss of NOESY cross-peak connectivity in the MPO strand was not immediately obvious. The DNA strand was not self-complementary, thus, based on the primary sequence, it should not self-associate or form a hairpin loop to maintain a stable structure. The chemical shifts of the cross-peaks in the base to H1′ region were similar across the temperature range, indicating that the duplex was stable throughout this "premelting" transition.

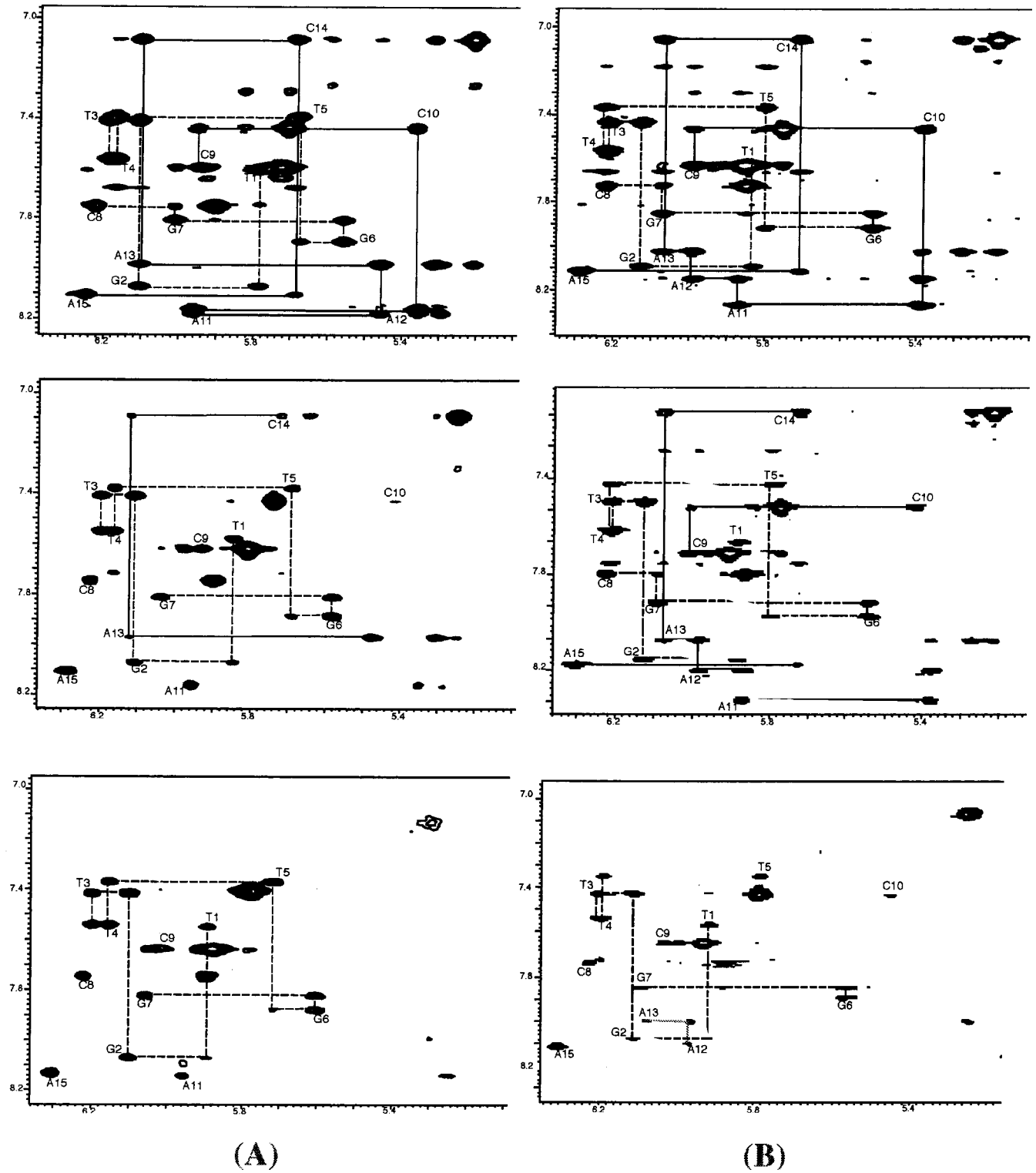

FIGURE 3: The H8 to H1′ region of the 2D NOESY spectra collected as a function of temperature. Column A: R_p isomer at 5 °C (top), 15 °C (middle), and 25 °C (bottom). Column B is S_p isomer at 5 °C (top), 15 °C (middle), and 25 °C (bottom). Dashed lines indicate connectivity for the DNA strand and the solid lines for the MP strand.

One explanation of the selective loss of NOESY connectivity in MPO strand was rapid exchange between several conformations of the MPO strand. The 5 °C NOESY data of the S_p isomer did show several extra low-intensity cross-peaks in the fingerprint (base to H1′ proton) region. These low-intensity cross-peaks were not observed in the NOESY data collected at higher temperatures (<15 °C).

Structure Calculations. Distance restraints obtained from integrating the NOESY volumes were used in the structure calculations using the iterative hybrid-matrix MORASS program. A total of 249 restraints were used for the R_p MPO duplex, and 243 restraints were used for the S_P MPO duplex. The quality of the refined structures was assessed by several key indicators, which are summarized in Table 3.

The 2D NOESY volumes calculated based on the final averaged structure fit very well with the experimental 2D NOESY volumes, indicating the high quality of the final structure and the refinement process. Significant deviations

Table 3: Structure Determination Statistics

	Rp isomer		Sp isomer	
	SA	⟨SA⟩[a]	SA	⟨SA⟩[a]
% RMS vol (exp)[b]	63.1	61.2 ± 4.8	91.6	89.3 ± 5.1
% RMS vol (the)[b]	74.5	71.8 ± 6.1	65.9	61.2 ± 6.5
R-factor[b]	0.3218	0.3213 ± 0.08	0.3682	0.3638 ± 0.08
Q(1/6) factor[b]	0.0667	0.0671 ± 0.007	0.0747	0.0764 ± 0.007
energy (total) (kcal/mol)	−329.6		−273.5	
energy (constraint) (kcal/mol)	60.8		55.1	
mean deviation from ideal covalent geometry				
bond angles (deg)		4.1		4.3
bond lengths (Å)		0.028		0.032
structure statistics				
distance violations				
>1.0 Å		0		0
>0.5 Å		1		2
>0.2 Å		16		22
distance restraints				
intraresidue		191		189
interresidue		138		132
hydrogen bond[c]		5		5

[a] ⟨SA⟩ Values for the 10 structures with lowest constraint energy. [b] For definitions see Materials and Methods. [c] Only one hydrogen bond restraint was used per base pair. No restraints were used for terminal base pairs.

between calculated and experimental NOESY volumes were seen for residues at the termini, where fraying of the strands and the resulting dynamics are not accounted for in the volume calculation. Though no dihedral restraints were used during the r-MD calculations, the sugar puckering and dihedral angles calculated for the final averaged structures agreed with the observations in 2D NOESY and the DQF−COSY spectra.

The stereoviews of the final averaged structures of the two isomers are shown in Figure 4, and an ensemble of 15 structures with lowest constraint energy is shown in Figure 5. The coordinates for the final structures are deposited at the Protein Data Bank.

DISCUSSION

Structural Features of the Heteroduplexes. The overall structures of the heteroduplexes are well defined as evidenced from the RMSD values and other parameters reported in Table 3. However, it should be noted that these structures are calculated based on experimental data collected at low temperatures (5 °C), and the structures of the duplexes are very dynamic at ambient temperatures. In the final structures of both heteroduplexes, the bases are very well stacked throughout the duplex. The observation of sequential aromatic-sugar proton NOESY cross-peaks for all residues in both strands supports the base-stacking arrangement. Calculated dihedral torsional angles and the results from the TOCSY and DQF−COSY data reveals that the sugars in the phosphodiester strand exhibit $C_{2'}$-endo sugar puckering while the sugars in the MPO strand are in an intermediate E-form exhibiting $C_{4'}$-endo sugar puckering. Stacking of bases on each other in the PD strand (even at higher temperatures) and the $C_{2'}$-endo sugar puckering show that the base-pairing with the MPO strands causes no major perturbation in the structure of the base-paired PD strand.

Evidence for Increased Dynamics in the MPO Strand. With an increase in temperature, an increase in line widths of the H2′/H2″ and H3′ signals was observed for the sugars in the MPO strand, whereas the line widths of sugars in the PD strand remain about the same. The unusual line broadening can be explained by higher dynamics of the MPO strand due to rapid transition between multiple conformers in the duplex. The deviation from $C_{2'}$-endo sugar puckering for sugars in the MPO strand also suggests that this strand might be experiencing higher dynamics compared to the PD strand.

The 2D NOESY collected as a function of temperature shows that the MPO strand undergoes some dynamic changes at higher temperatures, and the effect is more profound in the S_p isomer. The fact that at high temperatures the NOE cross-peak walk is disturbed in the MPO strand and not on the complementary DNA strand shows that the MPO strand is still bound to the complementary strand even at temperatures where few MP peaks remain. Sequential H8/H6 to H1′ connectivites were observed for the PD strand even at higher temperatures. The increased dynamics in the MPO strand may be due to the increased hydrophobicity of the phosphate backbone due to charge neutralization by the methyl substitution.

Differences in Hybridization Strength between the S_p and R_p Isomers. A change in chirality at a single phosphonate center in the MPO strand shows profound effect on its ability to hybridize with the target sequence, as evidenced from the 2D NOESY data presented here. Large-scale numerical simulations showed that the charge neutralization and the increased hydrophobicity of the phosphonate backbone significantly reduce the hydration of the phosphonate groups in MPOs (*49*). It is possible that the difference in the hybridization stability between the R_p and S_p MPOs may be due to the difference in the hydration of the phosphate backbone between the two isomers. The hydration is affected by the orientation of the methyl group that affects the accessibility to the major groove. In the R_p isomer, the methyl group protrudes from the helix into the solution away from the major groove, while in the S_p, the methyl group is oriented toward the major groove where unfavorable contacts occur. This orientation in the S_p could cause greater

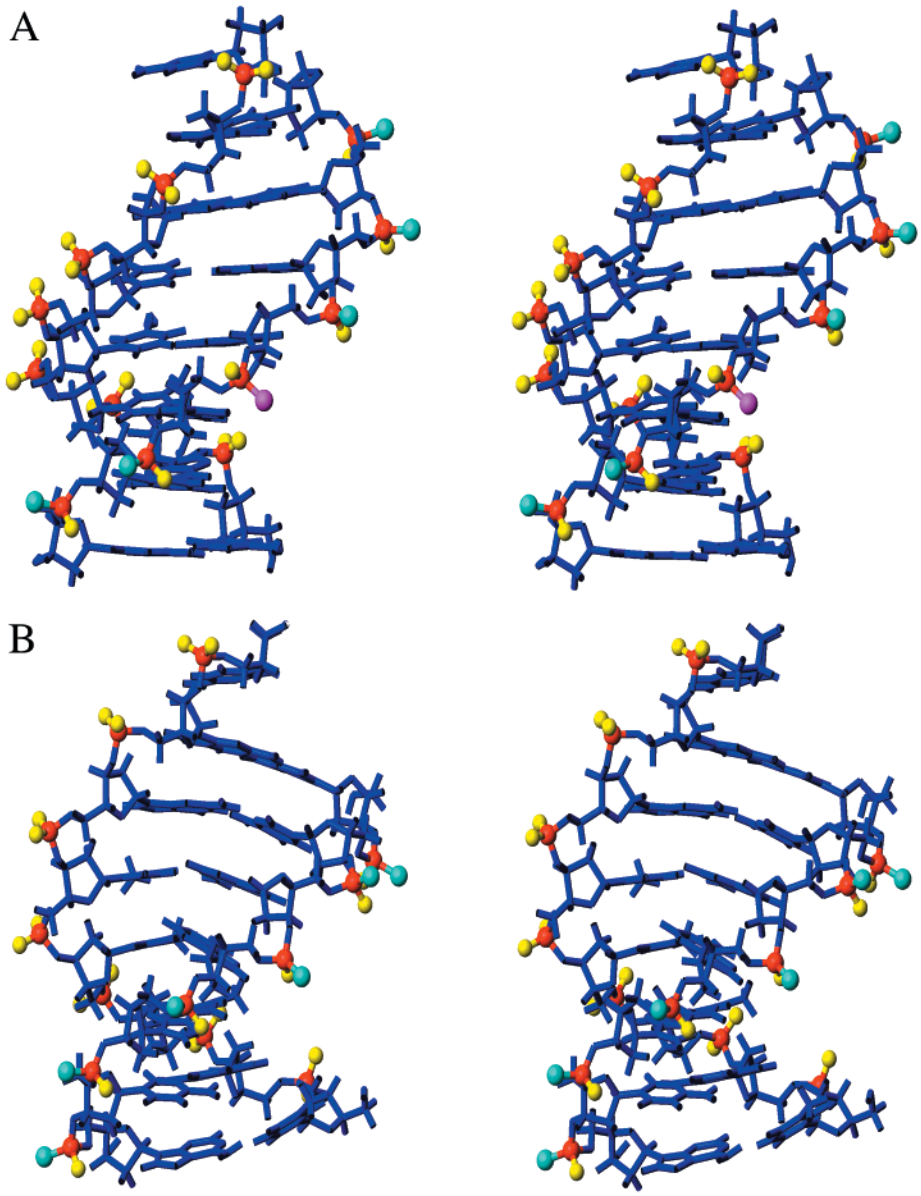

FIGURE 4: Final averaged structures of (A) S_p isomer and (B) R_p isomer heteroduplexes. The phosphorus atoms are shown in red, the nonbridging phosphoryl oxygens are in yellow, and the methyl groups of the phosphonate centers are in cyan.

disruption of the primary solvent shell and possibly reduce the number of water molecules that would normally surround the PD backbone (*49*).

The DQF spectra also showed that the furanose ring of residue A12 in the S_p isomer shows $C_{3'}$-endo sugar puckering, deviating from the rest of the sugars in the same strand. This remote conformational change in sugar puckering shows the destabilizing effect of the S_p substitution. In DNA and RNA duplexes, change in sugar ring puckering is often observed at perturbed sites [e.g., bulges in the helix (*50*)]. It is not certain whether the change in sugar puckering is a cause or a consequence of perturbation of the helix.

Another difference observed between the R_p and the S_p chiral centers is the phosphate conformation. For the S_p isomer, a distinct downfield ^{31}P signal was observed for the A13 phosphonate. In PD DNA, such shifts are interpreted as a tendency of P−O3′ torsions to assume more trans (extended B_{II}) conformations (*48*). Theoretical calculation revealed that the presence of S_p introduces a certain amount of restriction to the phosphodiester P−O3′ rotation, resulting in the increase in the barrier for possible transitions between B_I and B_{II} type transitions (*18*).

The results from this study clearly establish that the heteroduplex formed by the chirally pure R_p MPO is more stable than that formed with the MPO with one S_p chiral center. Substitution of more R_p centers with S_p centers will further destabilize the binding of the MPO strand to the target DNA/RNA strand. Theoretical calculations revealed that the Gibbs free energy change for hybridization, $\Delta\Delta G_{hybrid}$, of a single R_p to S_p perturbation in the MPO:DNA duplex is 3.6 kcal/mol (*49*). Therefore, to be used as effective antisense and antigene therapeutic agents, it is preferable to make chirally pure MPOs with R_p phosphonate center.

Strauss et al. (*51*, *52*) show that a racemic MPO mixed MP/phosphate duplexes are ~30% less bent in solution (as measured electrophoretically) than pure R_p MPO mixed duplexes. This indicated that S_p bends more than R_p since the racemic mixture contains both R_p and S_p MP centers. However, as these authors note, the electrophoretic band for the racemate is not broader than the pure R_p MPO mixed

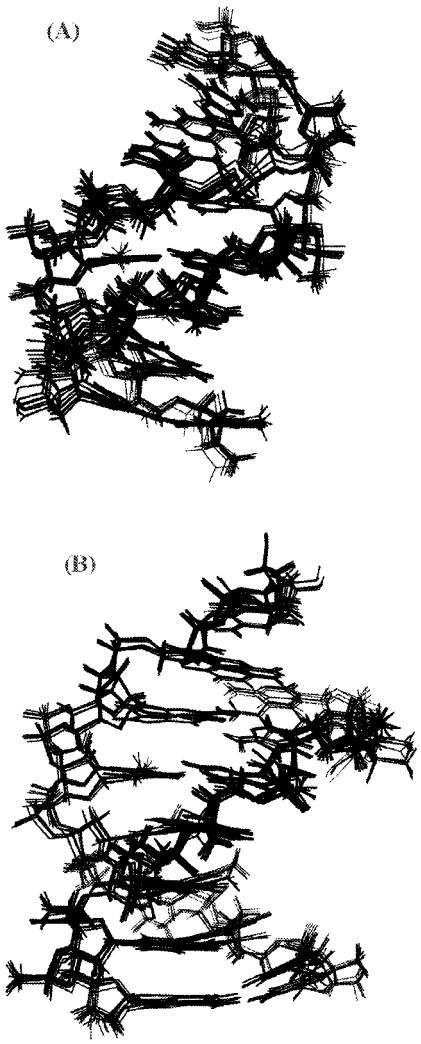

FIGURE 5: Overlay of 15 final structures with lowest constraint energy for (A) S_p isomer and (B) R_p isomer.

duplexes. This could be explained by the increased dynamics of the S_p duplex as shown in our present study. These duplexes represent time-averaged structures, and the S_p contains a higher population of bent duplexes. Strauss et al. suggested that the mixed MPO DNA duplexes are bent predominantly through an asymmetric charge neutralization (bending toward neutral MP patches). Our results suggest that in addition bending is also a dynamic effect introduced by the helix destabilizing S_p isomers.

Role of Metal Ions in Structural Perturbations. The minor groove width (P−P separation) for both hetero duplexes was found to be generally wider (Figure 6), varying between 12.3 and 15.0 Å for the R_p isomer and 11.4 and 13.8 Å for the S_p isomer) compared to the minor groove in B-form PD DNA (11.5 Å). According to the electrostatic model proposed by Wilson et al. (*53*), minor groove width is dramatically influenced by the coordination of monovalent cations within the minor groove. The groove appears to widen as ions move away from the minor groove and narrow as they move closer. Due to the presence of the bulky, neutral methyl groups in the phosphonate backbone, there would be lesser interactions between the Na^+ ions and the phosphate backbone resulting in the widening of the minor groove.

Significantly, the minor groove width differs substantially between the R_p and S_p isomers, particularly at the phosphonate diastereomeric center at residue 13. As shown in Figure 6, the minor groove width (P−P separation) is widest (15.0 Å) for the R_p isomer but is narrowest for the S_p isomer (11.4 Å) at this position. While in the R_p isomer the methyl group is oriented toward the solvent, it is also pointed toward the minor groove. For the S_p isomer the phosphoryl group is oriented toward the minor groove. One explanation (in addition to the solvation argument previously discussed) for these differences could simply be the greater steric bulk of the methyl group oriented toward the solvent/minor groove in the R_p isomer. Alternatively, if sodium or other cations are indeed bound in the minor groove as supported by recent X-ray (*54*−*56*), NMR (*57*), and calculational (*53*, *58*) studies of normal backbone duplex oligonucleotides, then only in the case of the S_p isomer could the phosphoryl group of the phosphonate help coordinate a metal ion across the minor groove to a phosphate on the opposing strand. Because the R_p and S_p isomers only differ at a single phosphonate center, with all of the others being the same R_p stereochemistry, this single site has a profound effect not only on the P−P separation at site 13 but at all of the others as well. Thus, at the other positions, the minor groove of the S_p isomer is 0.5−1.0 Å narrower than the R_p isomer, even though the stereochemistry of the phosphonates is the same at these other sites. This cooperative effect can be rationalized in terms of preferential binding of a metal ion into the S_p minor groove only.

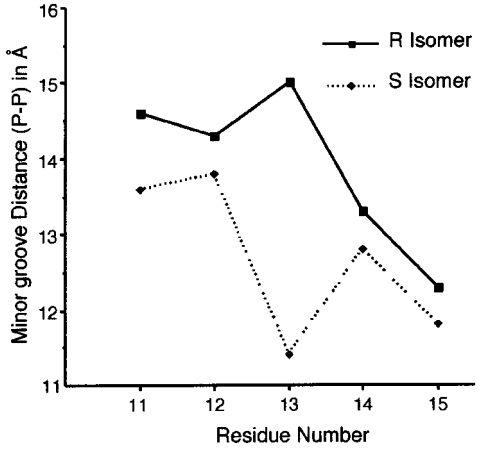

FIGURE 6: Plot of the minor groove distances measured between the phosphorus atoms across the minor groove.

In support of the important role of bound metal ions in defining the structure of duplexes (*53*−*58*) and in particular the minor groove width, we have recently completed the structures of several duplexes with multiple substitutions of dithiophosphates for normal backbone phosphates (D. Volk et al., unpublished). Like the methyl phosphonates, the minor grooves are considerably expanded, especially when two dithioates are opposed across the minor groove. Dithioates coordinate metal ions such as sodium ions much poorer than phosphates, and this increase in minor groove width (P−P separation increasing from 11.5 to 14 Å) is such to convert a normal B-form duplex to one with A-like character. The subject of the importance of bound metal ions is still controversial (*59*), and studies of backbone-modified oligonucleotides such as the MPOs may prove critical in understanding these perturbations.

Perhaps the fluxional nature of binding metal ions into the minor groove of the S_p isomer is also responsible for

the greater dynamics of the S_p strand than the R_p strand. It is clear that besides steric, electrostatic, and solvent interaction effects that are believed to contribute to the structural perturbations and increased stability of the R_p diastereomer, we need to be more aware of the important role played by specifically coordinated metal ions in these structures.

ACKNOWLEDGMENT

We wish to thank Dr. Irina G. Shishkina for preparation of the complementary DNA Lichrosorb support.

REFERENCES

1. Miller, P. S., Yano J., Yano, E., Carroll, C., Jayraman, K., and Ts'o, P. O. P. (1979) *Biochemistry 18*, 5134−5143.
2. Miller, P. S., Dreon, N., Pulford, S. M., and McParland, K. (1980) *J. Biol. Chem. 255*, 9659−9665.
3. Agraval, S., and Goodchaild, J. (1987) *Tetrahedron Lett. 28*, 3539−3542.
4. Agris C. H., Blake, K. R., Miller P. S., Reddy M. P., and Ts'o, P. O. P. (1986) *Biochemistry 25*, 6268−6275.
5. Miller, P. S., McParland, K. B., Jayraman, K., and Ts'o, P. O. P. (1981) *Biochemistry 20*, 1874−1880.
6. Jayraman, K., McParland, K., Miller, P. S., and Ts'o P. O. P. (1981) *Proc. Natl. Acad. Sci. U.S.A. 78*, 1573−1541.
7. Smith, C. C., Aurelian, L., Reddy, M. P., Miller, P. S., and Ts'o, P. O. P. (1986) *Proc. Natl. Acad. Sci. U.S.A. 83*, 2787−2791.
8. Chang E. H., Miller, P. S., Cushman, C., Devadas, K., Pirollo, K. F., Ts'o, P. O. P., and Yu, Z. P. (1991) *Biochemistry 30*, 12055−12061.
9. Blake, K. R., Murakami, A., Spitz, S. A., Glave, S. A., Reddy, M. P., Ts'o, P. O. P., and Miller, P. S. (1985) *Biochemistry 24*, 6139−6145.
10. Spiller D. G., Giles, R. V., Broughton, C. M., Grzybowski, J., Ruddell, C. J., Tidd, D. M., and Clark, R. E. (1998) *Antisense Nucleic Acid Drug Dev. 4*, 281−293.
11. Reynolds, M. A., Arnold, L. J., Almazan, M. T., Beck, T. A., Hogrefe, R. I., Metzler, M. D., Stoughton, S. R., Tseng, B. Y., Trapane, T. L., Ts'o, P. O. P., and Woolf, T. M. (1994) *Proc. Natl. Acad. Sci. U.S.A. 91*, 12433−12437.
12. Pritcharfd C. E., Grasby, J. A., Hamy, F., and Zacharek, A. M. (1994) *Proc. Natl. Acad. Sci. U.S.A.* 22, 2592−2600.
13. Smith, S. A., and McLaughlin, L. A. (1997) *Biochemistry 36*, 6046−6058.
14. Reynolds, M. A., Hogrefe, R. I., Jaeger, J. A., Schwartz, D. A., Riley, T. A., Marvin, W. B., Daily, W. J., Vagnefi, M. M., Beck, T. A., Knowles, S. K., Klem, R. E., and Arnold, L. J. (1996) *Nucleic Acids Res. 24*, 4584−4591.
15. Lesnikowski, Z. J., Jaworska, M., and Stec, W. J. (1990) *Nucleic Acids Res. 18*, 2109−2115.
16. Bower, M., Summers, M. F., Powell, C., Shinozuka, K., Regan, J. B., Zon, G., and Wilson, W. D. (1987) *Nucleic Acids Res. 15*, 4915−4930.
17. Fergusan, D. A., and Kollman, P. A. (1993) *Antisense Res. Dev. 1*, 243−254.
18. Swarnalatha, Y., and Yathindra, N. (1991) *J. Biomol. Struct. Dyn. 9*, 613−631.
19. Wozniak, L. A., Pyzowski, J., Wiezorek, M., and Stec, W. J. (1994) *J. Org. Chem. 59*, 5843−5846.
20. Schell, P., and Engles, J. W. (1998) *Tetrahedon Lett. 39*, 8629−8632.
21. Vyazovkina, E. V., Savchenko, E. V., Lokhov, S. G., Engels, J. W., Wickstrom, E., and Lebedev A. V. (1994) *Nucleic Acid Res. 22*, 2404−2409.
22. Chacko, K. K., Linder, K., Saenger, W., and Miller, P. S. (1983), *Nucleic Acid Res. 11*, 2801−2814.
23. Han, F., William, W., Duchamp, D. J., Callahan, L., Kezdy, F. J., and Agarwal, K. (1990) *Nucleic Acid Res. 18*, 2759−2769.
24. Mujeeb, A., Reynolds, M. A., and James, T. L. (1997) *Biochemistry 36*, 2371−2379.
25. Kanaori, K., Tamura, Y., Wada, T., Nishi, M., Kanehara, H., Morii, T., Tajima, K., and Makino, K. (1999) *Biochemistry 38*, 16058−16066.
26. Cho, Y., Zhu, F., Luxon, B. A., and Gorenstein, D. G. (1993) *J. Biomol. Struct. Dyn. 11*, 685−702.
27. Bichenkova, E. V., Abramova, T. V., Vorobev, Y. N., Zarytova, V. F., Ivanova, E. M., Maltseva, T. V., and Leberev, A. V. (1991) Nucleic Acids, in *Synthetic Oligonucleotides: Problems and Frontiers of Practical Application* (Knorre, D. G., Efimov, V. A., and Chakhmakhcheva, O. G., Eds.) pp 115−116, Symposium Series No. 24, IRL/Oxford University press, Oxford.
28. Miller, P. S., Reddy, M. P., Murakami, A., Blake, K. R., Lin, S., and Agris, C. H. (1986) *Biochemistry 25*, 5092−5097.
29. Vyazovkina, E. V., Rife, J. P., Lebedev, A. V. and Wickstrom, E. (1993) *Nucleic. Acids Res. 21*, 5957−5963.
30. Vyazovkina, E. V., Engels, J. W., and Lebedev, A. V. (1993) *Bioorg. Khim. 19*, 197−206.
31. Lebedev, A. V., Vyazovkina, E. V., Frauendorf, A., and Engels, J. W. (1993) *Tetrahedron 49*, 1043−1052.
32. Stec, W. J., Wozniak, L. A., Pyzowski, J., and Niewiarowski, W. (1997) *Antisense Nuc. Acid Drug Dev. 7*, 381−395.
33. Hogrefe, R. I., McCaffrey, A. M., Borozdina, L. I., McCampbell, E. S., and Vaghefi, M. M. (1993) *Nucleic Acids Res. 21*, 4739−4741.
34. States, D. J., Haberkorn, R. A., and Ruben, D. J. (1982) *J. Magn. Reson. 48*, 286−292.
35. Piantini U., Sorenson, O. W., and Ernst, R. R. (1982) *J. Am. Chem. Soc. 104*, 6800−6801.
36. Case, D. A., Pearlman, D. A., Caldwell, J. W., Cheatham, T. E., Ross, W. S., Simmerling, C. L., Darden, T. A., Merz, K. M., Stanton, R. V., Cheng, A. L., Vincent, J. J., Crowley, M., Ferguson, D. M., Radmer, R. J., Seibel, G. L., Singh, U. C., Weiner, P. K., and Kollman, P. A. (1997) AMBER5.0, University of California, San Francisco.
37. Jorgensen, W. L., Chandrasekkar, J., and Madura, J. D. J. (1983) *J. Chem. Phys. 79*, 926−935.
38. Cheatham, T. E., and Kollman, P. A. (1996) *J. Mol. Biol. 259*, 434−444.
39. Essmann, U., Perera, L., Berkowitz, M. L., Darden, T., Lee, H., and Pedersen, G. (1995) *J. Chem. Phys. 103*, 8577−8593.
40. Post, C. B., Meadows, R. P., and Gorenstein, D. G. (1990) *J. Am. Chem. Soc. 112*, 6796−6803.
41. Meadows, R., Post, C. B., Luxon, B. A., and Gorenstein, D. G. (1997) MORASS Program University of Texas Medical Branch, Galveston, TX.
42. Mujeeb, A., Kerwin, S. M., Kenyon, G. L., and James, T. L. (1993) *Biochemistry 32*, 13419−13431.
43. Thomas P. D., Basus, V. J., and James, T. L. (1991) *Proc. Natl. Acad. Sci. U.S.A. 88*, 1237−1241.
44. Nielsen, P. E., Egholm, M., Berg, R. H., and Buchardt, O. (1991) *Science 254*, 1497−1500.
45. Wüthrich, K. (1986) *NMR of Proteins and Nucleic Acids*, Wiley, New York.
46. Varani, G., and Tinoco, I., Jr. (1991) *Q. Rev. Biophys. 24*, 479−532.
47. Furrer, P., Billeci, T. M., Donati, A., Kojima, C., Karwowski, B., Sierzchala, A., Stec, W., and James, T. L. (1999) *J. Mol. Biol. 285*, 1609−1622.
48. Gorenstein, D. G., Luxon, B. A., Goldfield, E. M., Lai, K., and Vegeais, D. (1982) *Biochemistry 21*, 580−589.
49. Hausheer, F. H., Rao, B. G., Saxe, J. D., and Singh, U. C. (1992) *J. Am. Chem. Soc. 114*, 3201−3206.
50. Thiviyanathan, V., Guliaev, A. B., Leontis, N. B., and Gorenstein, D. G. (2000) *J. Mol. Biol. 300*, 1143−1154.
51. Strauss-Soukup, J. K., Vaghefi, M. M., Hogrefe, R. I., and Maher, L. J. (1997) *Biochemistry 36*, 8692−8698.
52. Strauss-Soukup, J. K., Rodrigues, P. D., and Maher, L. J. (1998) *Biophys. Chem. 72*, 297−306.
53. Hamelberg, D., McFail-Isom, L., Williams, L. D., and Wilson, W. D. (2000) *J. Am. Chem. Soc. 122*, 10513−10520.
54. Tereshko, V., Minasov, G., and Egli, M. (1999) *J. Am. Chem. Soc. 121*, 3590−3595.

55. Woods, K. K., McFail-Isom, L., Sines, C. C., Howerton, S. B., Stephens, R. K., and William, L. D. (2000) *J. Am. Chem. Soc. 122*, 1546−1547.
56. Sines, C. C., McFail-Isom, L., Howerton, S. B., van Derveer, D., and William, L. D. (2000) *J. Am. Chem. Soc. 122*, 11048−11056.
57. Hud, N. V., Sklenar, V., and Feigon, J. (1999) *J. Mol. Biol. 286*, 651−660.
58. Young, M. A., Jayaram, B., and Beveridge, D. L. (1997) *J. Am. Chem. Soc. 119*, 59−69.
59. Chiu, T. K., Grzeskowiak, M., and Dickerson, R. E. (1999) *J. Mol. Biol. 292*, 589−608.

BI011551K